Femtosecond ultraviolet laser absorption spectroscopy for simultaneous measurements of temperature and OH concentration

Cite as: Appl. Phys. Lett. **120**, 201103 (2022); https://doi.org/10.1063/5.0091572 Submitted: 16 March 2022 • Accepted: 03 May 2022 • Published Online: 16 May 2022

[ົ]ll Ning Liu, [™] Timothy Y. Chen, [™] Hongtao Zhong, et al.







ARTICLES YOU MAY BE INTERESTED IN

Laser terahertz emission microscopy of nanostructured spintronic emitters Applied Physics Letters 120, 201102 (2022); https://doi.org/10.1063/5.0080397

Enhanced optoelectronic performance and photogating effect in quasi-one-dimensional BiSel wires

Applied Physics Letters 120, 201101 (2022); https://doi.org/10.1063/5.0080334

Enhancing the efficiency of the topological phase transitions in spin-orbit photonics Applied Physics Letters 120, 181102 (2022); https://doi.org/10.1063/5.0086930

Lock-in Amplifiers up to 600 MHz









Femtosecond ultraviolet laser absorption spectroscopy for simultaneous measurements of temperature and OH concentration

Cite as: Appl. Phys. Lett. **120**, 201103 (2022); doi: 10.1063/5.0091572 Submitted: 16 March 2022 · Accepted: 3 May 2022 · Published Online: 16 May 2022







Ning Liu,^{1,a)} (b) Timothy Y. Chen,^{1,2} (b) Hongtao Zhong,¹ (b) Ying Lin,¹ (b) Ziyu Wang,¹ (b) and Yiguang Ju¹ (b)

AFFILIATIONS

¹Department of Mechanical and Aerospace Engineering, Princeton University, Princeton, New Jersey 08544, USA

ABSTRACT

This Letter reports a femtosecond ultraviolet laser absorption spectroscopy (fs-UV-LAS) for simultaneous *in situ* measurements of temperature and species. This fs-UV-LAS technique was demonstrated based on $X^2\Pi$ - $A^2\Sigma^+$ transitions of OH radicals near 308 nm generated in low temperature plasmas and flames. The fs-UV-LAS technique has revealed three major diagnostic benefits. First, a series of absorption features within a spectral bandwidth of \sim 3.2 nm near 308 nm were simultaneously measured and then enabled simultaneous multi-parameter measurements with enhanced accuracy. The results show that the temperature and OH concentration could be measured with accuracy enhanced by 29–88% and 58–91%, respectively, compared to those obtained with past two-narrow-line absorption methods. Second, an ultrafast time resolution of \sim 120 picoseconds was accomplished for the measurements. Third, due to the large OH $X^2\Pi$ - $A^2\Sigma^+$ transitions in the UV range, a simple single-pass absorption with a 3-cm path length was allowed for measurements in plasmas with low OH number density down to \sim 2 × 10¹³ cm⁻³. Also due to the large OH UV transitions, single-shot fs absorption measurements were accomplished in flames, which was expected to offer more insights into chemically reactive flow dynamics.

Published under an exclusive license by AIP Publishing. https://doi.org/10.1063/5.0091572

Recently, femtosecond (fs) lasers have attracted tremendous attention across a wide variety of laser diagnostics for combustion and plasma, since it can generate pulses that feature femtosecond timescale in the time domain and broadband spectrum in the frequency domain. The feature of femtosecond timescale can be utilized to explore ultrafast chemistry¹ (e.g., chemical decomposition²) with fs to picosecond (ps) time resolution. The feature of broadband spectrum can be utilized to develop various ultrafast laser diagnostics, such as fs/ps coherent anti-stokes Raman spectroscopy, ^{3,2,7} fs two-photon absorption laser induced fluorescence, ⁴ fs mid-infrared laser absorption spectroscopy (LAS), ⁵ fs laser electronic excitation tagging, ⁶ and fs electric field induced second harmonic generation. ⁷

This Letter focuses on the use of broadband nature of fs lasers for laser absorption spectroscopy. Currently, the typical commercial fs lasers feature a bandwidth of tens to hundreds cm⁻¹ [significantly larger than those of many past narrow-line methods, ^{10–12} e.g., tunable diode laser absorption spectroscopy (TDLAS) with external cavity diode lasers] in the frequency domain and also a pulse duration of tens to hundreds fs in the time domain. ^{8,9} These two features can offer

two corresponding benefits to the absorption techniques. First, the broadband of fs lasers can enable multi-parameter/species measurements with enhanced accuracies. The broadband can be used to simultaneously sense many transitions of single/multiple species with different dependences on target parameters, leading to multi-species/parameter measurements. Also, these measured transitions can serve as constraints in the absorption fitting and provide more independent information to reduce the uncertainties (e.g., due to multi-species line overlaps) of simultaneous multi-parameter/species measurements. Second, the fs laser pulse duration inherently enables a fs or ps time resolution. Such time resolution is considerably shorter than those of many past methods with, e.g., continuous-wave (CW) or nanosecond (ns) lasers, which are largely limited to microsecond (μ s) or ns time resolution. This benefit will further extend the application of fs laser absorption to ultrafast chemistry.

With the above understanding, this Letter reports a direct fs ultraviolet laser absorption spectroscopy (fs-UV-LAS) for temperature and species measurements. The fs-UV-LAS was demonstrated based on the $X^2\Pi\text{-}A^2\Sigma^+$ transitions of hydroxyl (OH) radicals near 308 nm

²Presently at Sandia National Laboratories, Livermore, California 94550, USA

a) Author to whom correspondence should be addressed: nl7@princeton.edu

in low temperature plasmas (LTPs) and flames. The OH radical was selected for demonstrating fs-UV-LAS, because it represents one of the key species in reactive flows, and its $X^2\Pi$ - $A^2\Sigma$ ⁺ band experiencing marginal interferences from other species is appropriate for broadband absorption. Essentially, fs-UV-LAS exhibits three diagnostic benefits. First, many absorption features within ~3.2 nm near 308 nm were simultaneously measured and then provided to the absorption fitting. With abundant features as constraints, temperature and OH concentration can be simultaneously measured with accuracies enhanced significantly by 29-88% and 58-91%, respectively, compared to those from past methods as shown later. Second, an ultrafast time resolution of \sim 120 ps was enabled in the measurements. Third, with the large OH $X^2\Pi$ - $A^2\Sigma$ ⁺ transitions, a simple single-pass absorption configuration was possible for measurements in LTPs featuring low OH number density down to $\sim 2 \times 10^{13} \, \text{cm}^{-3}$. By contrast, such low OH number density would set up a roadblock to single-pass absorption using the infrared (IR) transitions of OH, which are at least two orders of magnitude weaker than its UV transitions. Also with the large OH UV transitions, single-shot fs-UV-LAS measurements were enabled in flames as demonstrated later.

The experiment designed to demonstrate fs-UV-LAS for simultaneous $in\ situ$ measurements of temperature and OH concentration in LTPs is shown in Fig. 1. This setup consists of a fs laser system, a plasma reactor, a spectrometer, and a camera. The fs laser system (Coherent Astrella) combining a Ti:Sapphire oscillator, an ultrafast amplifier, and an optical parametric amplifier (OPA, Light Conversion TOPAS NirUVIS) was used to generate the fs UV laser pulses. Specifically, the Ti:Sapphire oscillator and the ultrafast amplifier were used to generate the laser pulses centered at 800 nm with a pulse duration of 80 fs at a repetition rate of 1 kHz. Then, these laser pulses were converted by the OPA into the UV pulses with a bandwidth of \sim 3.2 nm near 308 nm and a pulse energy of 38 μ J.

The fs UV laser pulses then entered a plasma reactor and was absorbed by the $X^2\Pi$ - $A^2\Sigma^+$ transitions of OH radicals generated in plasmas. The plasma reactor was largely similar to that detailed in Ref. 13, 28 and 29 with only one difference on the electrodes resulting in a plane-to-plane discharge. Two short cylindrical electrodes with a gap distance of 5 mm were fixed in parallel at the reactor center. The electrodes were made of stainless steel, and one of them was covered by dielectric material, i.e., quartz of 1.63 mm thickness. Each cylindrical electrode had a diameter of 30 mm (i.e., the absorption path length) and a height of 5.5 mm, and their edges were smoothed to prevent the

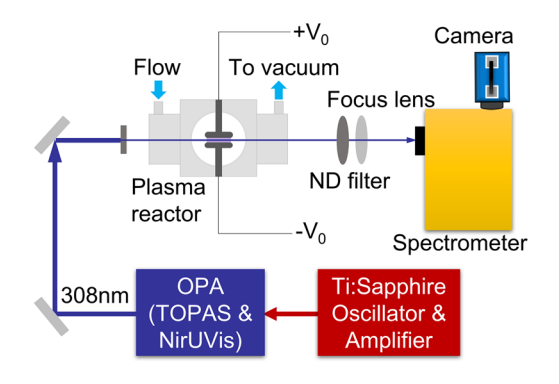


FIG. 1. Experimental setup for fs-UV-LAS in LTPs.

electric field concentration. These two electrodes were connected to a ns voltage pulser (FID GmBH FPG 30-50MC4). The ns pulser operated repetitively in a burst mode with a burst frequency of 2 Hz, under which the plasma volume could be fully flushed with new gas between two consecutive bursts. Each burst had 200-1500 pulses operated at a 30-kHz rate, and each pulse had a 6-kV peak voltage and a 12-ns pulse duration. Each repetitive plasma discharge burst was controlled by a delay generator (SRS DG645) with a fixed time after the laser pulse, and each burst was measured only once by one laser pulse. Therefore, the time resolution of end measurements, no matter single-shot or shot-averaged, was limited to the laser pulse time of flight through plasma and the time jittering of the delay generator totaling $\sim \! 120$ ps. Such ultrafast time resolution was beyond the capability of past absorption methods that were largely limited to μ s or ns time resolution. The gas mixture flowed into the reactor continuously, reacted in the plasma between two electrodes, and was then exhausted to vacuum. Two gas mixtures were used: (1) helium (He) with a flow rate of 900 sccm (standard cubic centimeter per minute) saturated with water (H2O) vapor maintained at 100 Torr and (2) methane (CH₄), oxygen (O₂), and He with rates of 100, 200, and 640 sccm, respectively, at 90 Torr. For the mixture (1), the water saturation was accomplished by passing the He flow through a water vessel maintained at \sim 40 °C by a heater. Under the above conditions, a steady plasma was generated with OH radicals uniformly distributed between two electrodes.

Then, the fs UV laser pulses were collected using a spectrometer (Acton SP2500i) and an intensified CCD camera (Princeton Instruments PIMAX-4 1024i). Specifically, the fs laser pulses were first attenuated by a neutral-density filter to avoid the camera CCD saturation and were then focused by a fused silica plano–convex lens (f= 200 mm) onto the slit (of 10 μ m width) of the spectrometer. The spectrometer equipped with a 2400 grooves/mm diffraction grating was adopted to spectrally disperse laser pulses. The dispersed pulses were then taken by the camera with an exposure time of 1 μ s. The camera was synchronized with the fs laser and ns voltage pulser using the delay generator. With this spectrometer-camera system, each pixel on the camera CCD along the horizontal direction corresponded to a wavelength of 0.009 nm. The pixels were vertically binned to improve the signal-to-noise ratio (SNR).

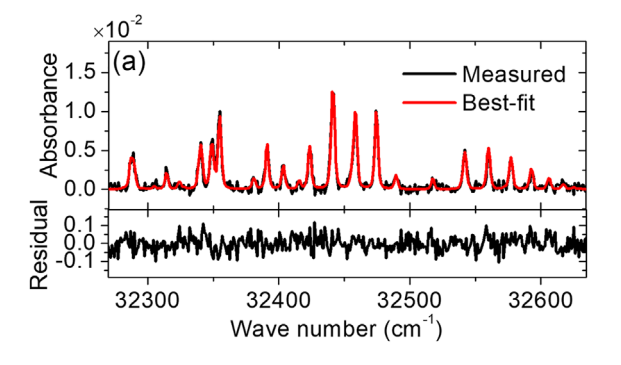
With the above setup, the baseline and transmitted laser spectrum intensities $I_0(\nu)$ and $I_t(\nu)$ (with regard to the wave number ν) were captured with the plasma off and on, respectively. The background noises were captured with the plasma off and on to correct the $I_0(\nu)$ and $I_t(\nu)$, respectively. Then, the measured $I_0(\nu)$ and $I_t(\nu)$ after background corrections were input into a spectral fitting method to infer temperature and OH concentration. The spectral fitting method was similar to that described in Ref. 5, and it inferred temperature and OH by fitting the calculated absorbance spectrum to the measured absorbance based on the Beer–Lambert law as formulated as follows:

$$\ln\left(I_t(\nu)/I_0(\nu)\right) = \sum_i S_i(T)\phi_i(\nu)P\chi L,\tag{1}$$

where $\ln(I_i(\nu)/I_0(\nu))$ is the absorbance, T is the temperature, $S_i(T)$ is the ith T-dependent line-strength, $\phi_i(\nu)$ is the line shape function, P is the pressure, χ is the mole fraction (i.e., concentration) of the absorber (i.e., OH), and L is the absorption path length (i.e., 30 mm). The fitting was performed in four steps. The first step initialized temperature and OH concentration, which were then used to calculate the absorbance

spectrum as formulated on the righthand side of Eq. (1) and the HITRAN database. The second step obtained the calculated $I_{t,c}(\nu)$ with $I_0(\nu)$ and the calculated absorbance from step 1. In this step, the instrument response function (IRF) of the spectrometer-camera system was used as a convolution kernel to broaden $I_{t,c}(v)$. The IRF was modeled as a Voigt profile with FWHM (full width at half magnitude) as the resolution (i.e., 0.0287 nm, calculated theoretically based on grating dispersion and also verified experimentally within measurement accuracy) of the spectrometer-camera system and with the relative weight between the Gaussian and Lorentzian components to be fitted. The third step calculated the instrumentally broadened absorbance spectrum $\ln(I_{t,c}(\nu)/I_0(\nu))$. The fourth step iteratively compared $\ln(I_{t,c}(\nu)/I_0(\nu))$ to the measured absorbance $[\ln(I_t(\nu)/I_0(\nu))]$ and solved for the temperature and OH concentration using a nonlinear least squares algorithm. 14,30,31 The above introduced the experimental setup and data processing where noise was inevitable. Supplementary material 1 analyzed the main noise sources and summarized the counter measures to reduce the noise and improve the SNR.

Next, fs-UV-LAS measurements were performed on both H_2O/He and $CH_4/O_2/He$ plasmas. Figure 2(a) first shows a sample shotaveraged fs-UV-LAS result on the H_2O/He plasma at the end of 200 voltage pulses in the pulse burst. Figure 2(a) compares the measured OH absorbance $[\ln(I_t(\nu)/I_0(\nu))$ after background correction] against the best-fit absorbance. The measured absorbance was obtained by averaging 250 shots separately taken on 250 plasma bursts and, hence, showed a SNR of \sim 8:1. The best-fit absorbance was obtained using the spectral fitting. As seen, the best-fit absorbance agreed well with the measured absorbance with a residual within 1.2×10^{-3} . With this fit,



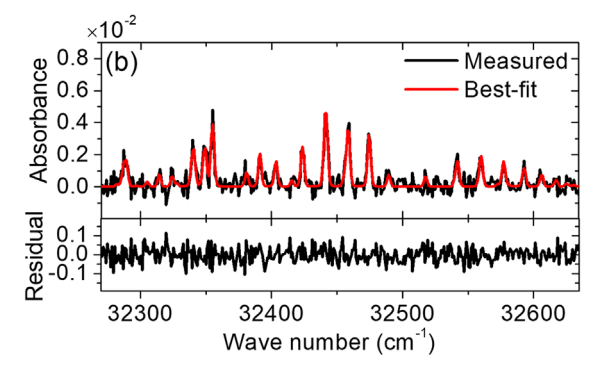


FIG. 2. Sample shot-averaged fs-UV-LAS measurements along with the spectral fits on the (a) H_2O/He plasma and (b) $CH_4/O_2/He$ plasma.

the temperature was determined to be 334.8 K, while the OH mole fraction was determined to be 59.3 ppm (parts per million). In parallel, Fig. 2(b) shows another shot-averaged sample fs-UV-LAS result for the CH₄/O₂/He plasma produced at the end of 1500 voltage pulses in the burst. The measured absorbance averaged 400 shots separately on 400 plasma bursts, providing a SNR of \sim 4:1. As seen, the best-fit absorbance was in good agreement with the measured absorbance with a residual within 1.1×10^{-3} . The temperature and OH mole fraction extracted from the fit were 418.7 K and 31.9 ppm, respectively.

To demonstrate the single-shot capability of fs-UV-LAS in reactive flows, we also performed experiments on hot flames where the OH concentration was high enough to enable single-shot measurements. The flame setup was largely similar to the plasma setup as shown in Fig. 1 with one difference: The plasma reactor was replaced with a Bunsen burner. The burner generated the premixed laminar stoichiometric propane-air flame under atmospheric pressure. The single-shot fs-UV-LAS measurements were performed horizontally through the central region of the flame and near the flame tip. Figure 3 shows the sample single-shot fs-UV-LAS measurement with the fit on the flame. The laser shot-to-shot variation was corrected based on the a priori information that the absorbance spectrum portion without any absorption feature theoretically equaled zero. As seen, the fs-UV-LAS OH spectrum in the flame illustrated the singleshot capability and exhibited a good SNR of \sim 9:1. The temperature and OH mole fraction were fitted to be 1780.1 K and 722.9 ppm on average (due to the line-of-sight integration nature of absorption), respectively. This single-shot measurement featured an ultrafast time resolution of \sim 100 ps (limited to the laser pulse time of flight through the flame).

The above experiments demonstrated fs-UV-LAS for simultaneous temperature and OH measurements with ultrafast time resolution in LTPs and also its single-shot capability in flames. Next, simulations were performed to further illustrate the advantages of fs-UV-LAS in accuracy enhancement over past methods. Beyond the experiments, simulations can provide the ground truth for the target temperature and OH concentration (which was difficult to be known *a priori* experimentally) as well as the target absorption spectrum, such that the accuracies of both temperature and OH can be quantified. The simulations employed three sets of published temperature and OH results by past narrow line absorption methods with tunable CW lasers from 15–17 as ground truth. These ground truth results are summarized in the supplementary material 3, Fig. S1, and they can be used to comprehensively validate fs-UV-LAS in enhancing accuracy,

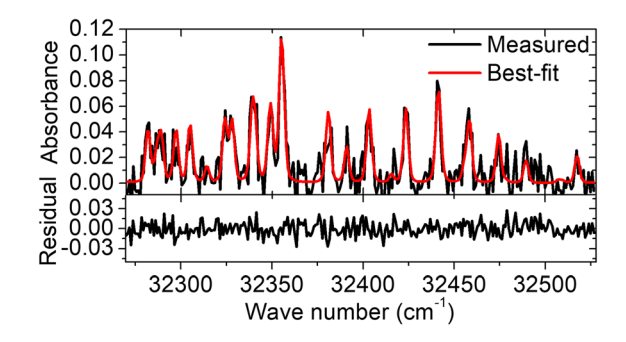
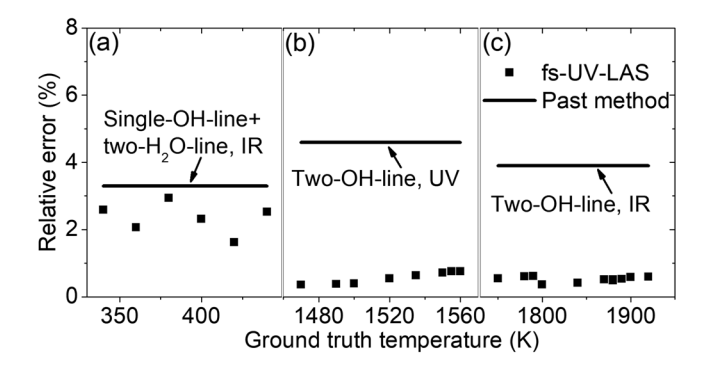


FIG. 3. Sample single-shot fs-UV-LAS measurement with the fit on the flame.

because they represent most reactive flow applications from three perspectives: (1) absorbance of fs-UV-LAS that considerably affects the final accuracy that ranges from \sim 0.01 to \sim 0.7; (2) application scenarios from plasmas to flames; and (3) various past methods for comparisons, e.g., the two-UV-absorption-line method and two-IR-absorption-line method. Along with the ground truth, past work also quantified accuracies, which could be directly used to elucidate the accuracy enhancement by fs-UV-LAS. The simulation procedure consisted of a forward problem and an inverse problem as detailed in the supplementary material 2. The forward problem involved synthesizing $I_0(\nu)$ and $I_t(\nu)$ based on the ground truth temperature and OH concentration. The inverse problem involved spectrally fitting the synthetic $I_0(\nu)$ and $I_t(\nu)$ and solving for the temperature and OH, which were then compared against the ground truth results for accuracy quantifications.

Figure 4 illustrates the advantage of fs-UV-LAS in enhancing accuracy over past methods. Figures 4(a)–4(c) show the comparisons of temperature accuracies between fs-UV-LAS and past methods using simulations based on three sets of published data, while Figs. 4(d)–4(f) show the comparisons of OH concentration accuracies. As shown in Fig. 4(a), fs-UV-LAS could significantly reduce the measurement error of temperature by 29% to 2.3% on average, compared to 3.3% obtained using the past method that combined single OH line with two H_2O lines in IR in a ns discharge plasma featuring a small absorbance of \sim 0.01 (\sim 10¹³ cm⁻³ in OH number density) and strong inherent electromagnetic interference (EMI) besides other common noises (e.g., laser shot noise and detector noise). This significant error



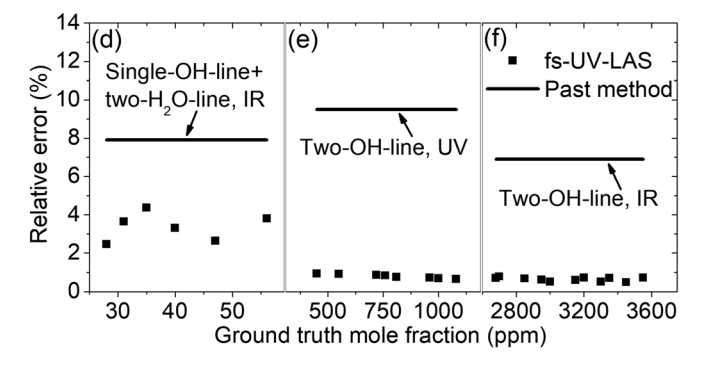


FIG. 4. Comparison of fs-UV-LAS and past methods using simulations on the accuracies of (a)–(c) temperature and (d)–(f) OH concentration.

reduction was offered by the broadband sensing of fs-UV-LAS. The error reduction could be amplified when fs-UV-LAS was tested on hot flames with large absorbance (e.g., 0.1-0.7) as shown in Figs. 4(b) and 4(c). As seen, fs-UV-LAS reduced the temperature error by 88% to 0.56% on average compared to 4.6% obtained by a past method using two OH lines in UV, and also by 86% to 0.51% on average compared to 3.9% by a two-OH-IR-line method. Similar observation can also be made on the OH comparisons shown in Figs. 4(d)-4(f). As shown in Fig. 4(d), fs-UV-LAS reduced the OH concentration error by 58% to 3.3% on average compared to 7.9% from the hybrid OH/ H₂O-IR-line method with temperature obtained from two H₂O lines in plasmas with low OH number density. Also, as shown in Figs. 4(e) and 4(f), fs-UV-LAS substantially reduced the OH error by 91% to 0.8% on average in comparison with 9.5% from the two-OH-UV-line method, and also by 90% to 0.65% in comparison with 6.9% from the two-OH-IR-line method. Along with the above comparisons, supplementary material 3 and 4 summarized more detailed results and provided more insights into the fs-UV-LAS capability of improving accuracies of simultaneous measurements. Before leaving the discussion, two points regarding accuracy are noteworthy. First, although this work only showed three sets of comparisons, the fs-UV-LAS accuracies still outperformed other published accuracies on OH and/or temperature measurement under similar conditions (i.e., absorbance and noise), e.g., the results in Figs. 4(b), 4(c), 4(e), and 4(f) vs the \sim 1%–3% errors in Refs. 18–22. Second, the accuracies of both temperature and OH by fs-UV-LAS shown in Figs. 4(b), 4(c), 4(e), and 4(f) were comparable to or even higher than many TDLAS temperature and/or major species measurements using two or more lines, such as CH_4^5 and H_2O^{23-25} with $\sim 1\%$ errors under similar conditions.

Finally, one note is worth mentioning. Admittedly, the use of spectrometer in fs-UV-LAS introduced extra spectrum broadening that might impair the detection limit to some extent. However, we argue that it is still valuable for two reasons. First, using spectrometer could provide many absorption features to dramatically improve the accuracy. Second, as illustrated above, even with the spectrometer, fs-UV-LAS could still detect OH down to $2\times10^{13}\,\mathrm{cm}^{-3}$, which covers most combustion and plasma applications. In the future, the fs-UV-LAS signal collection can be upgraded by replacing the spectrometer and camera with a long dispersive fiber and a photodiode, 26 and the resulting chirped signal can map the spectral features in time with marginal instrument broadening.

In summary, this work reported fs-UV-LAS for simultaneous in situ measurements of temperature and species in LTPs and also demonstrated its single-shot capability in flames. The measurements were based on OH $\rm X^2\Pi$ -A $^2\Sigma^+$ transitions. The fs-UV-LAS shows three major benefits over previous methods: (1) simultaneous temperature and OH measurements with significantly enhanced accuracies, (2) the ultrafast time resolution of \sim 120 ps, and (3) the simple single-pass absorption configuration for the measurements with low OH number density down to \sim 2 × 10 13 cm $^{-3}$, and the single-shot capability that would further extend fs-UV-LAS to the study of combustion/ flow/plasma dynamics.

See the supplementary material for (1) experimental noise sources and the associated counter measures, (2) the detailed simulation procedure, (3) the detailed OH concentration and temperature comparisons between ground truth and inferred results using simulations,

and (4) the example fs-UV-LAS fits used to obtain temperatures and OH concentrations.

Funding is provided by NSF (No. CBET-1903362), NSF EFRI (No. DCheM-2029425), DOE grant of Plasma Science Center (No. DE-SC0020233), ExxonMobil research grant, and DOE NETL grant (No. DEFE0026825).

AUTHOR DECLARATIONS

Conflict of Interest

The authors have no conflicts to disclose.

DATA AVAILABILITY

The data that support the findings of this study are available from the corresponding author upon reasonable request.

REFERENCES

- ¹H. Xu, Y. Cheng, S. L. Chin, and H. B. Sun, Laser Photonics Rev. **9**, 275–293 (2015).
- ²V. Apatin, V. Kompanets, V. Laptev, Y. A. Matveets, E. Ryabov, S. Chekalin, and V. Letokhov, Chem. Phys. Lett. 414, 76–81 (2005).
- ³T. L. Courtney, N. T. Mecker, B. D. Patterson, M. Linne, and C. J. Kliewer, Appl. Phys. Lett. **114**, 101107 (2019).
- ⁴W. D. Kulatilaka, J. R. Gord, V. R. Katta, and S. Roy, Opt. Lett. **37**, 3051–3053 (2012).
- ⁵R. J. Tancin, Z. Chang, M. Gu, V. Radhakrishna, R. P. Lucht, and C. S. Goldenstein, Opt. Lett. 45, 583–586 (2020).
- ⁶Y. Zhang and R. B. Miles, Opt. Lett. **43**, 551–554 (2018).
- ⁷B. M. Goldberg, T. L. Chng, A. Dogariu, and R. B. Miles, Appl. Phys. Lett. **112**, 064102 (2018).
- ⁸S. Yalcin, Y. Wang, and M. Achermann, Appl. Phys. Lett. **93**, 101103 (2008).
- ⁹H. U. Stauffer, P. S. Walsh, S. A. Schumaker, and S. Roy, Optica 7, 847–853 (2020).
- ¹⁰S. Johnson, Y. Ding, D. Davidson, and R. Hanson, Combust. Flame 238, 111962 (2022).
- ¹¹L. Dong, C. Li, N. P. Sanchez, A. K. Gluszek, R. J. Griffin, and F. K. Tittel, Appl. Phys. Lett. 108, 011106 (2016).

- ¹²A. Muraviev, D. Maukonen, C. Fredricksen, G. Medhi, and R. Peale, Appl. Phys. Lett. 103, 091111 (2013).
- ¹³T. Y. Chen, B. M. Goldberg, B. D. Patterson, E. Kolemen, Y. Ju, and C. J. Kliewer, Opt. Lett. 45, 4252–4255 (2020).
- ¹⁴T. F. Coleman and Y. Li, SIAM J. Optim. **6**, 418–445 (1996).
- ¹⁵A. Rousso, X. Mao, Q. Chen, and Y. Ju, Proc. Combust. Inst. 37, 5595–5603 (2019).
- ¹⁶M. Donovan, D. Hall, P. Torek, C. Schrock, and M. Wooldridge, Proc. Combust. Inst. 29, 2635–2643 (2002).
- ¹⁷T. Aizawa, Appl. Opt. **40**, 4894–4903 (2001).
- ¹⁸T. N. Anderson, R. P. Lucht, T. R. Meyer, S. Roy, and J. R. Gord, Opt. Lett. 30, 1321–1323 (2005).
- ¹⁹S. S. Vasu, Z. Hong, D. F. Davidson, R. K. Hanson, and D. M. Golden, J. Phys. Chem. A **114**, 11529–11537 (2010).
- ²⁰ K. Y. Lam, D. F. Davidson, and R. K. Hanson, Int. J. Chem. Kinet. 45, 363–373 (2013).
- ²¹P. Bruggeman, G. Cunge, and N. Sadeghi, Plasma Sources Sci. Technol. 21, 035019 (2012).
- ²²Q. Xiong, Z. Yang, and P. J. Bruggeman, J. Phys. D 48, 424008 (2015).
- ²³ A. Farooq, J. B. Jeffries, and R. K. Hanson, Meas. Sci. Technol. 19, 075604 (2008).
- ²⁴S. Li, A. Farooq, and R. K. Hanson, Meas. Sci. Technol. 22, 125301 (2011).
- 25 X. Liu, J. Jeffries, R. Hanson, K. Hinckley, and M. Woodmansee, Appl. Phys. B 82, 469–478 (2006).
- ²⁶N. G. Blume and S. Wagner, Opt. Lett. **40**, 3141–3144 (2015).
- ²⁷T. Y. Chen, N. Liu, C. J. Kliewer, A. Dogariu, E. Kolemen, and Y. Ju, "Simultaneous single-shot rotation-vibration non-equilibrium thermometry using pure rotational fs/ps CARS coherence beating," Opt. Lett. 47(6), 1351–1354 (2022).
- ²⁸N. Liu, H. Zhong, Y. Lin, T. Y. Chen, T. Z. Wang, and Y. Ju, "OH concentration and temperature measured by femtosecond cavity enhanced absorption spectroscopy in a nanosecond-pulsed dielectric barrier discharge," in AIAA SCITECH 2022 Forum (2022) p. 1946.
- ²⁹T. Chen, N. Liu, A. Dogariu, E. Kolemen, and Y. Ju, "Rotation-vibration non-equilibrium measurement using pure rotational fs/ps CARS coherence beating," in AIAA SCITECH 2022 Forum (2022) p. 2123.
- ³⁰N. Liu and L. Ma, "Hybrid diagnostic for optimizing domain size and resolution of 3D measurements," Opt. Lett. 43(16), 3842–3845 (2018).
- ³¹N. Liu, Q. Lei, Y. Wu, Y., and L. Ma, "3D tomography reconstruction improved by integrating view registration," Appl. Opt. 58(10), 2596–2604 (2019).